β-carboline alkaloid harmine induces DNA damage and triggers apoptosis by a mitochondrial pathway: study *in silico*, *in vitro* and *in vivo*

NÁDIA S.R.S. MOTA[1], MAICON R. KVIECINSKI[2], KARINA B. FELIPE[3],
VALDELÚCIA M.A.S. GRINEVICIUS[1], TÂMILA SIMINSKI[1], GABRIELA M. ALMEIDA[1],
RODRIGO C. ZEFERINO[1], CLAUS T. PICH[4], DANILO W. FILHO[5] and ROZANGELA C. PEDROSA[1]

[1]Department of Biochemistry, Federal University of Santa Catarina (UFSC), Florianópolis, SC 88040-900;
[2]Postgraduate Program of Health Sciences (PPGCS), University of Southern Santa Catarina (UNISUL),
Palhoça, SC 88137-270; [3]Department of Clinical Analysis, Federal University of Paraná (UFPR), Curitiba,
PR 80060-000; [4]Center for Sciences, Technologies and Health of the Araranguá Campus, Federal University
of Santa Catarina (UFSC) (UFSC), Araranguá, SC 88905-120; [5]Department of Ecology and Zoology,
Federal University of Santa Catarina (UFSC) (UFSC), Florianópolis, SC 88040-900, Brazil

Abstract. Harmine, a tricyclic β-carboline alkaloid is an important metabolite present in *Passiflora incarnata* L. and *Passiflora edulis* f. *flavicarpa* Degener. Fruits of these plants are highly consumed in tropical countries and are popularly known as passion fruit, a natural product with potential anti-tumour activity. The cytotoxicity and selectivity effects were evaluated *in vitro* using tumour cell lines (MCF-7, HeLa) and normal mouse fibroblasts (McCoy cells). Molecular assays were performed using CT-DNA analysed by UV-Visible spectroscopy, fluorescence spectroscopy and circular dichroism, followed by *in silico* simulation (AutoDock Vina and GROMACS) and Comet assay. *In vivo* antitumour activity was assessed in Balb/c mice bearing Ehrlich ascitic tumour. Harmine presented cytotoxicity and selectivity to tumour cells. Spectrometry, molecular simulations and Comet assay suggested that harmine binds onto DNA nucleo base pairs by intercalation, consequently inducing DNA fragmentation. Furthermore, harmine decreased the PARP1-dependent DNA repair mechanism, causing cell cycle arrest in the G_2/M phase through inhibition of pRb phosphorylation and reduced expression of CDK2, cyclin A and cyclin B1. Moreover, harmine decreased mitochondrial membrane potential and caused mitochondrial-related cellular Bax-dependent and p53-independent apoptosis in MCF-7 cells. This β-carboline alkaloid also decreased tumour growth, body weight, volume of ascitic fluid and volume of packed tumour cells, while increased the non-viable/viable tumour cells ratio, which consequently increased the lifespan of animals bearing tumours. Mechanistically, our findings indicate a putative antitumor effect of harmine, which associates DNA damage, DNA repair repression, cell cycle arrest and triggering apoptosis through mitochondrial pathway. The results suggest that harmine, present in the pulp and seed of the passion fruit, could be used in future as a promising coadjutant anticancer agent and we suggest to address this fruit as a functional food.

Introduction

Despite advances in technology and medicine in terms of diagnosis and therapy, cancer is now the leading cause of death worldwide and thus remains a serious health issue and an economic burden (1). With the exception of non-melanoma skin cancer, prostate tumour is the most frequent cancer in men, while breast tumour is the most frequent cancer in women.

Tumour surgical excision, radiotherapy, immunotherapy and chemotherapy are the gold standard approaches for cancer treatment; however, current therapies still present critical points, mainly in terms of safety, efficacy and efficiency. The existing chemotherapy alternatives are often associated with non-complete tumour eradication and/or high toxicity and non-specificity. Additionally, several reports highlight a remarkable and crescent induction of cellular multiresistance to chemotherapeutic agents. Thus, there is a need to develop new alternative anticancer drugs with fewer side effects. One important strategy to develop effective anticancer agents relies on the study of bioactive compounds derived from natural

sources. Many of these, as well their derivatives, have been extensively studied and are proven to be effective for cancer prevention and therapy (2).

Alkaloids are nitrogenated pharmacologically active compounds, which have been reported to be one of the most important groups of phytocompounds obtained from natural sources (3). β-carbolines belongs to the group of indolic alkaloids (4). These alkaloids are mainly found in plants of the Zygophyllaceae, Malpighiaceae, Fabaceae, Myristicaceae, Elaeagnaceae and Passifloraceae families (5).

Harmine (7-methoxy-1methyl-9H-pyrido[3,4-b]indole), a tricyclic β-carboline alkaloid, was originally isolated from seeds of *Peganum harmala* L. (Zygophyllaceae) (6). However, there are also reports of this alkaloid as an important metabolite present in *Passiflora incarnata* L. and *Passiflora edulis* f.*flavicarpa* Degener, fruits of these plants are highly consumed in tropical countries and are popularly known as passion fruit or maracujá in the Brazilian indigenous language (6,7). The emphasis on the 'maracujá' fruit and seed is due to the extensive consumption of passion fruit juice (fresh or processed) and on ongoing investigations into its potential as a functional food. Many substances present in the fruits, mainly in the pulp and seed, can contribute to beneficial effects, such as antioxidant, anti-hypertension, as well as decreasing blood glucose and cholesterol. Commercial varieties of passion fruit are also rich in alkaloids, flavonoids, carotenoids, minerals and vitamins A and C, substances responsible for a variety of functional effects on other foods (8,9).

Previous studies have also shown that harmine have multiple pharmacological activities, including antiplasmodial, antileishmanial, antiviral, antimicrobial, anti-inflammatory and anticancer effects (6,10). *In vitro* studies have demonstrated that the planar structure of harmine leads to inhibition of topoisomerase activity (11). In addition, harmine has been shown to exert an anti-proliferative effect, in a dose and time-dependent manner, on several types of cancer cells, such as C33A, HL60, MGC-803, SW620 and SW480 cell lines (10,12).

Although previous studies have reported that β-carboline alkaloids can activate both the intrinsic and extrinsic pathways of apoptosis in tumor cells (13), the mechanisms of action of harmine are not fully elucidated. Therefore, the aim of this study was to perform biological screening for the antitumour activity of β-carboline alkaloid harmine and its interaction with DNA, using *in silico*, *in vitro* and *in vivo* models.

Materials and methods

Chemicals and antibodies. Agarose, propidium iodide (PI), acridine orange, calf thymus DNA (CT-DNA), tetrazolium salt (MTT), dimethylsulfoxide (DMSO), bovine serum albumin (BSA), tetramethylrhodamine methyl ester (TMRE), 5,5'-dithiobis(2-nitrobenzoic acid) (DTNB) and the protease inhibitor cocktail were purchased from Sigma-Aldrich; Merck KGaA. Antibiotics, Dulbecco's modified Eagle's medium (DMEM), Dulbecco's phosphate-buffered saline (PBS) and fetal bovine serum (FBS) were purchased from Gibco; Thermo Fisher Scientific, Inc. The kit of PI/ribonuclease A (RNAse) were acquired from Immunostep. Phosphatase inhibitor cocktail was purchased from Calbiochem (Merck Biosciences). Rabbit polyclonal antibodies raised against CDK2 (cat.

no. sc-163), cyclin A (cat. no. sc-596), cyclin B1 (cat. no. sc-752), PARP1 (cat. no. sc-7150), actin (cat. no. sc-7210) and mouse monoclonal antibodies raised against Bax (cat. no. sc-7480), Bcl-xL (cat. no. sc-8392) and p53 (cat. no. sc-126) were from Santa Cruz Biotechnology. Rabbit polyclonal antibody raised against phospho-Rb (cat. no. 9308) was acquired from Cell Signalling Technology. Polyclonal goat secondary antibodies for anti-rabbit IgG (cat. no. AP132P) and for anti-mouse IgG (cat. no. AP181P), as well as the chemiluminescence detection kit of HRP-coupled antibodies were from Merck Millipore. All other chemicals used were American Chemical Society (ACS) grade reagents.

Cell culture. Human breast carcinoma (MCF-7), cervix adenocarcinoma (HeLa) and normal mouse fibroblast (McCoy) cells were purchased from the Rio de Janeiro cell bank, Brazil. The cells were maintained at constant temperature (37˚C) under a 5% CO_2 atmosphere with 95% air humidity. The culture medium used was DMEM supplemented with 10% FBS, penicillin (100 U/ml) and streptomycin (100 μg/ml).

Cytotoxicity assay. The cell viability was assessed using the MTT assay (14). Cells were plated at a density of $1x10^4$ cells/well in 96-well plates. After reaching 80% confluence, the cells were treated with different concentrations of harmine (0.1 to 1,000 μM) for 48 and 72 h. The negative control was treated only with standard culture medium containing 0.1% DMSO. After the treatment, cells were washed with PBS and incubated for 2 h with MTT (0.5 mg/ml). The formazan crystals were solubilized by adding DMSO (100 μl/well), and the colored solutions were read at 550 nm. Three independent experiments were conducted and the results are presented as the half maximal inhibition concentration (IC_{50}), calculated using Graph Pad Prism 6 (GraphPad Software Inc.). The selectivity index (SI) of the compounds under study are expressed as previously reported by Koch *et al* (15), with a minor modification: SI (selectivity index) = IC_{50} of the compound in a normal cell line/IC_{50} of the same compound in the cancer cell line.

Assessment of cell death type. The type of cell death induced by harmine was evaluated by a staining method, using PI and acridine orange (16). This method allows the differentiation of viable cells (green) from those that are dying through apoptosis (orange) or necrosis (dark red). MCF-7 cells were seeded ($2x10^5$/well) in 6-well plates. After confluence was reached, the cells were treated with IC_{30} and IC_{50} concentrations of harmine for 72 h. Fresh medium was used as a negative control. After treatment, the cells were stained with PI (100 mg/ml) and acridine orange (100 mg/ml) (5 μl; 1:1 v/v) and then visualized using an Olympus microscope, model BX41 (Olympus Corporation). Results are expressed as the percentages of cells that were viable, apoptotic or necrotic.

Mitochondrial membrane potential (MMP). Mitochondrial membrane depolarization was determined using the fluorescent probe, TMRE, which accumulates in the mitochondrial matrix in proportion to mitochondrial membrane potential ($\Delta\Psi$m) (17). MCF-7 cells were seeded at a density of $1x10^6$/well on 6-well plates. After confluence the cells were treated with IC_{30} and IC_{50} concentrations of harmine for 48 h. Thereafter,

the cells were incubated in the dark with TMRE (25 nM) for 20 min at 37°C. Cell fluorescence was determined using a BD FACS Canto II flow cytometer (BD Biosciences) and results are presented as the percentages of cells with high TMRE fluorescence.

Cell cycle distribution. The DNA content of the cells was measured by flow cytometry using a PI (50 μg/ml) and RNAse (0.2 mg/ml) solution kit. MCF-7 cells were seeded (2×10^5/well) in 6-well plates. After confluence was reached, the cells were synchronized using nocodazole (30 ng/ml) for 14 h and then treated with harmine (IC_{30}) for 72 h. Subsequently, the cells were fixed overnight with ethanol (70%) at -20°C, washed with a PBS/albumin (2%) solution, and later incubated with the PI/RNAse solution for 15 min at room temperature. The cells were evaluated using the BD FACS Canto II flow cytometer (BD Biosciences) and categorized into each phase of the cell cycle, according to the content of DNA. Flowing Software 2.5.0 (Perttu Terho; Cell Imaging Core, Turku Center for Biotechnology, University of Turku) was used to process the data.

DNA interaction and intercalation. The potential interaction of harmine with calf-thymus DNA (CT-DNA) was assessed through Spectrophotometric UV-Visible Scanning Titration (18). Increasing concentrations of harmine (0-250 μM) were used for an absorption titration assay with a constant concentration of CT-DNA (150 μM). To obtain the spectra of the samples, a Hitachi U-2910® spectrophotometer was used; and UV-Visible scanning was performed from 200 to 800 nm. The changes in CT-DNA absorbance, after incubation with harmine, as well as the maximum absorption wavelength shift, were determined.

Potential DNA intercalation was evaluated by fluorescence titration measurements, using the DNA-intercalating agent PI, according to Da Silveira *et al* (19). CT-DNA (150 μM) was saturated with PI (300 μM) in a phosphate buffer (50 mM) containing 0.1 M NaCl (pH 7.4). Increasing concentrations of harmine (0-250 μM) were then incubated with fixed concentrations of CT-DNA and PI for 10 min at room temperature. Doxorubicin, a standard antitumor intercalating drug, was used as a positive control. The SpectraMax Paradigma® Multileader was used to measure the variation of the sample fluorescence. Excitation and emission wavelengths of 492 and 620 nm were used, respectively.

The circular dichroism (CD) DNA interaction assay was performed as described by Bertoldo *et al* (20). The CD spectra were measured in a JASCO-810 spectropolarimeter (JASCO). A fixed concentration of CT-DNA (150 μM), prepared in a phosphate buffer (50 mM) containing 0.1 M NaCl (pH 7.4), was titrated with increasing concentrations of harmine to achieve a molar ratio of 0.04, 0.05 and 0.07 DNA/harmine. All CD spectra of DNA and DNA/harmine were recorded over the range of 220-350 nm and the final data were expressed in millidegrees (mdegs).

In silico study: DNA docking and molecular dynamic. The B-DNA template structure sequence d (CGTGAATTCACG) (PDB ID1G3X) was retrieved from Protein Data Bank (21). The ligand INE.mol2 file came from the ZINC database (http://zinc.docking.org/substance/18847046) and was minimized after removal of original co-precipitated ligands and water with UCSF Chimera 1.13 (22) using the AMBER99bsc1 force field (23). The ACPYPE tool, based on Python (24), was used as an Antechamber to generate INE topology for molecular simulations (25). Molecular docking simulations were applied to AutoDock MGLTools 1.5.6rc3 to generate a DNA-INE complex input file (.pdbqt) (26). Geometries and binding affinity energies were then calculated through AutoDock Vina 1.2.2 algorithm, using default parameters (27). H-bonds and/or hydrophobic interactions predicted between INE and DNA nucleotides were visualized with PyMOL open source 1.8.7.0' for Python 3.6 (28) and with LigPlot$^+$ 2.1 (29). However, subsequent molecular dynamic (MD) simulations used only the ligand pose (pdbqt) that had the lowest RMSD and binding affinity. Avogadro (30) was used to convert this file to .pdb format, before MD simulations with GROMACS version 2018.4 (31,32) using an AMBER99bsc1 force field (23). The TIP3P water model was applied in order to solvate and neutralize the system with two Na+ ions inside an octahedron box (33). The runs made for energy minimization and solvent equilibration kept grid space under NVP and NPT ensemble conditions (T=300 K, P=1 bar). All simulations used the same time step (1 fs). Position restricted heavy atoms of DNA accessible to the solvent, without disturbing the complex structure.

Molecular Mechanics Poisson-Boltzmann surface area (MM-PBSA) energies calculations. MM-PBSA calculations performed after MD simulations showed some conformational fluctuations and residue energy contributions for free binding energy (34). The MM-PBSA method calculated the energies and trajectories related to DNA and the ligand INE complex. This method, using explicit solvent, also enables the calculation of non-bonded potentials (electrostatic and van der Waals) under default parameters. Results were visualized with Visual Molecular Dynamics (VMD) (35) for LINUXAMD64, version 1.9.4a12 (2017). Calculations of trajectories used Verlet through MD neighbor searching and the vdW cutoff-scheme (36). Additionally, the 'readHBmap.py' (Python 2) program showed frames with H-bonds. Additionally, H bond occupancy graphics showed frames (1 frame equal to 2 ps) where this interaction contributed to the macromolecule - ligand complex stability (37). Finally, frames selected were visualized (Chimera and LigPlot$^+$ 2.1) and key intermolecular interactions between DNA-ligand were evaluated.

DNA damage. The DNA fragmentation was evaluated by the comet assay, according to Singh *et al* (38). MCF-7 cells were seeded (2.5×10^4/well) in 24-well plates. After confluence, the cells were treated with IC_{30} and IC_{50} concentrations of harmine for 72 h. After resuspending the cells in low-melting point agarose (0.75%), they were placed on slides pre-covered with agarose (1.5%) and incubated for 10 min at -8°C. The cells were then lysed for 7 days using the lysis solution (2.5 M NaCl; 10 mM Tris; 100 mM EDTA; 1% Triton X-100 and 10% DMSO; pH 10.0) and then submitted to horizontal electrophoresis (25 V and 300 mA) in alkaline buffer (300 mM NaOH; 1 mM EDTA; pH 13.0) for 20 min at 8°C. Subsequently, the slides were neutralized and fixed with the respective

solutions; neutralizing solution (0.4 M Tris HCl; pH 7.5) and fixing solution (15% TCA; 5% ZnSO$_4$; 5% glycerol). These procedures were intercalated with water washing. After drying at room temperature, the slides were stained (0.1% NH$_4$NO$_3$, 0.1% AgNO$_3$, 0.25% tungstosilicic acid, 0.15% formaldehyde, 5% Na$_2$CO$_3$, v/v), washed with acetic acid (0.01%) and visualized on an Olympus microscope, model BX41 (Japan). The comets were classified according to Ross *et al* (39), in which the score 0 represented the undamaged nuclei and a score of 4 represents maximally damaged nuclei.

Western blotting. MCF-7 cells were treated with the IC$_{30}$ concentration of harmine for 48 h and then washed with PBS and lysed in RIPA buffer (50 mM Tris-HCl, pH 7.4; 150 mM NaCl; 1% NP40; 0.25% Na-deoxycholate and 1 mM phenyl-methylsulfonyl fluoride), supplemented with protease inhibitor (1%) and phosphatase inhibitor (3%) cocktails. Laemmli buffer (60 mM Tris-HCl, 2% sodium dodecyl sulphate (SDS), 10% glycerol, 5% β mercaptoethanol and 0.01% bromophenol blue, pH 6.8) was used to denature the proteins. Subsequently, 25 μg of denatured protein were submitted to sodium dodecyl sulphate-polyacrylamide gel electrophoresis (SDS-PAGE), followed by electrotransfer to polyvinylidene fluoride (PVDF) membranes (40). Following blocking and washing, the membranes were incubated with the primary antibodies overnight at - 8°C (Rabbit polyclonal antibodies raised against phospho-Rb (1:1,000, v/v), CDK2 (1:1,000, v/v), cyclin A (1:1,000, v/v), cyclin B1 (1:1,000, v/v) and PARP1 (1:1,000, v/v); Mouse monoclonal antibodies raised against Bax (1:200, v/v), Bcl-xL (1:200, v/v) and p53 (1:200, v/v). Lastly, the membranes were washed and incubated with secondary antibodies for at least 1 h. The polyclonal goat anti-rabbit IgG antibody (1:5,000, v/v) and polyclonal goat anti-mouse IgG antibody (1:3,000, v/v) are both peroxidase conjugated. A chemiluminescence detection kit for HRP-coupled antibodies was used for immunodetection. Actin (1:1,000, v/v) was used as a loading control. Images acquired (ChemiDoc MP System; Bio-Rad Laboratories, Inc.) were normalized with actin.

In vivo antitumour activity. The antitumor activity of harmine was evaluated using male Balb/c mice (20±2 g, n=12) kept under controlled conditions (12 h light-dark cycle, 22±2°C, 60% air humidity), receiving water and food *ad libitum*. Previous tests were done to select the maximal safe dose of harmine with the optimal dilution and the doses of 10 mg/kg/day and 20 mg/kg/day were chosen to continue the experiments. The induction of Ehrlich ascitic carcinoma (EAC) was carried out according to a method previously reported by Kviecinski *et al* (41). Before tumour induction, all mice were weighed (g) and their abdominal circumferences (cm) were measured. The mice were then inoculated intraperitoneally with EAC cells (5x10^6 cells/200 μl). After 24 h, the animals were divided into 4 groups (n=12). The negative control group was treated with saline containing 1% DMSO. The positive control group received doxorubicin (0.6 mg/kg/day) as previously reported (42). Test groups received harmine at 10 or 20 mg/kg/day, respectively. The treatments were administered intraperitoneally for 9 consecutive days. Twenty-four hours later, all mice were weighed and their abdominal circumferences measured again. Using the

formula reported by Felipe *et al* (43), the inhibition (%) of tumour growth was calculated as follow: [(variation in waist circumference of the treated group x 100)/variation in waist circumference of the control group] - 100. The variation in body weight of the treated animals was calculated as reported by Kviecinski *et al* (41): Final weight (after 9 days of treatment) - Initial weight (day zero, day of tumour inoculation). Then, the animals (n=12) were kept alive and assisted on a daily basis to evaluate survival (lifespan), according to Kaplan and Meier (44). Lastly, the treatment was repeated and the animals were euthanised after 9 days of treatment. The ascitic fluid was collected in graduated falcon conical tubes and centrifuged at 5,000 x g for 5 min to measure packed tumour cells volume (41). Viability of the tumour cells was assessed through the trypan blue assay (45).

Statistical analyses. All *in vitro* assays were performed in technical triplicates, whereas the *in vivo* experiments were performed in biological replications (n=12; α=0.05; Power (1 - β)=0.90; critical t=1.81; df (degree of freedom)=10; Effect size |ρ|=0.67). The results were presented as means ± standard deviations or as percentages. Data were analysed using analysis of variance one-way ANOVA followed by the Bonferroni post-hoc test or log-rank test, when necessary. Comparisons were performed using the software GraphPad Prism 6 (GraphPad Software Inc.). P<0.05 was considered to indicate a statistically significant difference.

Results

Harmine is cytotoxic with selectivity to tumour cells. The cytotoxic effect of β-carboline alkaloid harmine was evaluated against two tumour cell lines (MCF-7 and HeLa) and a normal cell line (McCoy). The values obtained for the IC$_{50}$ and SI for harmine in 48 and 72 h are shown in Fig. 1A. Harmine significantly decreased tumour cell viability in a time and dose-dependent manner (Fig. 1B and C). Additionally, harmine showed selectivity for all tumour cell lines tested (Fig. 1A) and it is worth noting that this alkaloid presented the highest selectivity for MCF-7 cells (SI=4.44).

Harmine induces predominantly apoptosis and modulates the expression of Bcl-2 and p53 proteins. Results indicated that harmine was able to induce significant cell death (Fig. 2A) and the numbers of apoptotic cells in the presence of this alkaloid (27.88 and 46.47 μM) were significant. However, only the concentration of 46.47 μM harmine caused an increase in necrotic cells (8.67±3.47%), when compared to the negative control (1.81±0.70%). Also, harmine (46.47 μM) decreased the number of viable cells by approximately 32.9% while increasing the number of apoptotic (82.3%) and necrotic (79.1%) cells, compared to the negative control.

The modulators effects of harmine on pro- and anti-apoptotic proteins were investigated by exposing MCF-7 cells to harmine (27.88 μM) for 48 h. Fig. 2C and D show that harmine increased the expression of Bax protein, while reducing the expression of Bcl-xL protein. Accordingly, the Bax/Bcl-xL ratio was significantly increased when MCF-7 cells were treated with harmine, suggesting cell death through apoptosis via the mitochondrial pathway. However, harmine induced
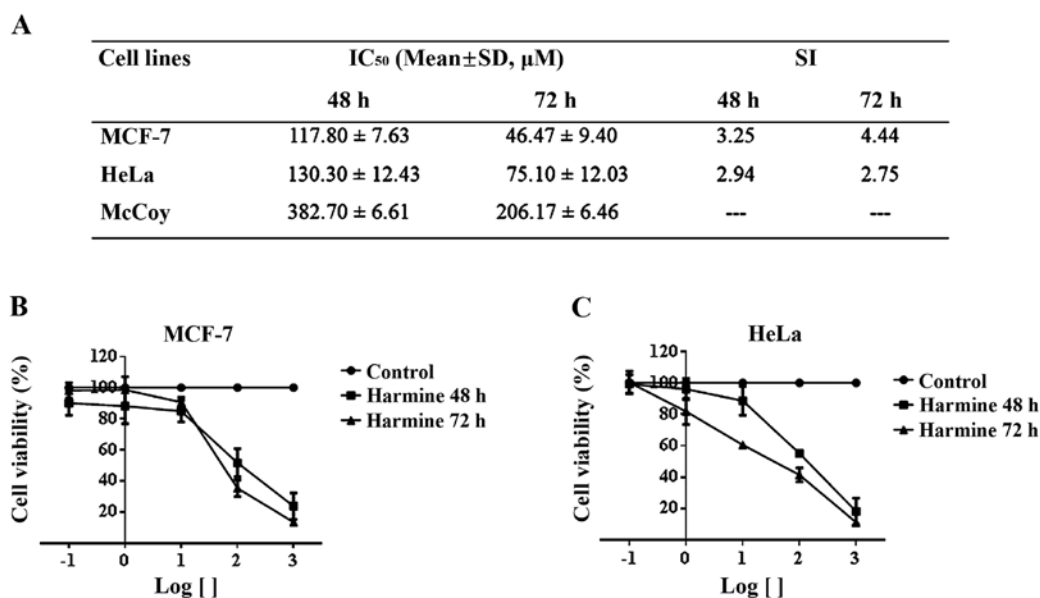
A

Cell lines	IC$_{50}$ (Mean±SD, μM)		SI	
	48 h	72 h	48 h	72 h
MCF-7	117.80 ± 7.63	46.47 ± 9.40	3.25	4.44
HeLa	130.30 ± 12.43	75.10 ± 12.03	2.94	2.75
McCoy	382.70 ± 6.61	206.17 ± 6.46	---	---

Figure 1. (A) Cytotoxicity and selectivity of harmine on MCF-7, HeLa and McCoy cells after 48 and 72 h of treatment (0.1, 1, 10, 100 and 1,000 μM) evaluated by the MTT assay. Dose-time-response curves of (B) MCF-7 and (C) HeLa cells treated with harmine. Results are expressed as the means ± standard deviation of three independent experiments. IC$_{50}$ values were obtained using the Software GraphPad Prism 6.0 (GraphPad Software Inc.). IC$_{50}$, half maximal effective concentration; SI, selectivity index.

apoptotic cell death independently of p53, since MCF-7 cells show underexpression of this pro-apoptotic protein (Fig. 2C and E).

Harmine induces mitochondrial membrane depolarization. Our results showed that harmine induced a dose-dependent depletion of ΔΨm in the MCF-7 cells (Fig. 2B). At concentrations of 27.88 and 46.47 μM harmine showed a ΔΨm of 79.65±1.85 and 72.26±2.41%, respectively, whereas the negative control was 85.45±3.08%. Thus, harmine at the concentration of 46.47 μM was capable of decreasing the ΔΨm of MCF-7 cells by 15.4%, when compared to the negative control.

Harmine induces cell cycle arrest through inhibition of phosphorylation of pRb and decreases expression of CDK2, cyclin A and B1. Fig. 3A and B show the changes in the MCF-7 cell cycle after treatment with harmine. Cells from the negative control had 65.50±0.96, 13.41±1.03 and 21.01±1.59% of cells in G$_1$, S and G$_2$/M phase, respectively. The treated cells presented 67.70±0.85, 3.53±0.58 and 26.12±0.38% of cells in G$_1$, S and G$_2$/M phase, respectively. Harmine (27.88 μM) promoted a significant decrease (73.7%) in the number of cells in the S phase and a significant increase (approximately 19.6%) in the number of cells in the G$_2$/M phase, when compared with the negative control. However, MCF-7 cells treated with harmine was not statistically different in relation to the number of cells in G$_1$ phase, when compared to untreated cells, suggesting a G$_2$/M arrest of cells. In addition, after the treatment there was an increase of cells in the sub-G$_1$ area (2.67±0.11%), compared to the negative control (0.08±0.08%), which is indicative of cell death through apoptosis, confirming the previous result (Fig. 2A).

Treatment of MCF-7 cells with harmine (27.88 μM) for 48 h totally inhibited the phosphorylation of pRb (Fig. 3C and D). Additionally, harmine caused a significant decrease in the expression of cell cycle proteins, CDK2, cyclin A and cyclin B1 (Fig. 3C and D), which may explain the significant reduction of cells present in the S phase and cell cycle arrest at the G$_2$/M phase (Fig. 3A and B).

Harmine interacts with CT-DNA. Firstly, the interaction between harmine and CT-DNA was analysed by spectrophotometric UV-visible scanning titration, causing both hypochromic and bathochromic effects (Fig. 4A); thereby suggesting that β-carboline alkaloid binds to DNA by intercalation.

In order to find further evidence of the intercalative interaction of harmine with CT-DNA, spectrophotometric titrations were carried out using the DNA-intercalating agent, PI. When the concentration of harmine was increased (Fig. 4B), PI fluorescence decreased, suggesting that harmine succeed in intercalating between the nucleobase pairs of DNA and to displace PI bound to DNA, consequently causing a reduction in the fluorescence intensity of the sample.

CD was also employed to gain insight into the DNA conformational alterations that occur after harmine was bound to DNA. A typical CD spectrum of CT-DNA in its B form shows a positive band with a maximum at 275 nm, due to base stacking, and a negative band with a minimum at 248 nm, due to right-handed helicity (46). Therefore, alterations in the B-DNA secondary structure lead to a change in the CD spectrum (47). Our results showed that harmine was able to induce changes in the CD spectrum by increasing the intensity of the negative and the positive bands of CT-DNA (Fig. 4C). Accordingly, the CD spectrum results from the DNA-harmine complex were consistent with those of the intercalation model.

In silico prediction. Molecular docking and dynamic studies of the binding model of harmine with DNA were used to gather further structural details of the DNA-harmine complex. The pose that had the lowest binding energy, predicted
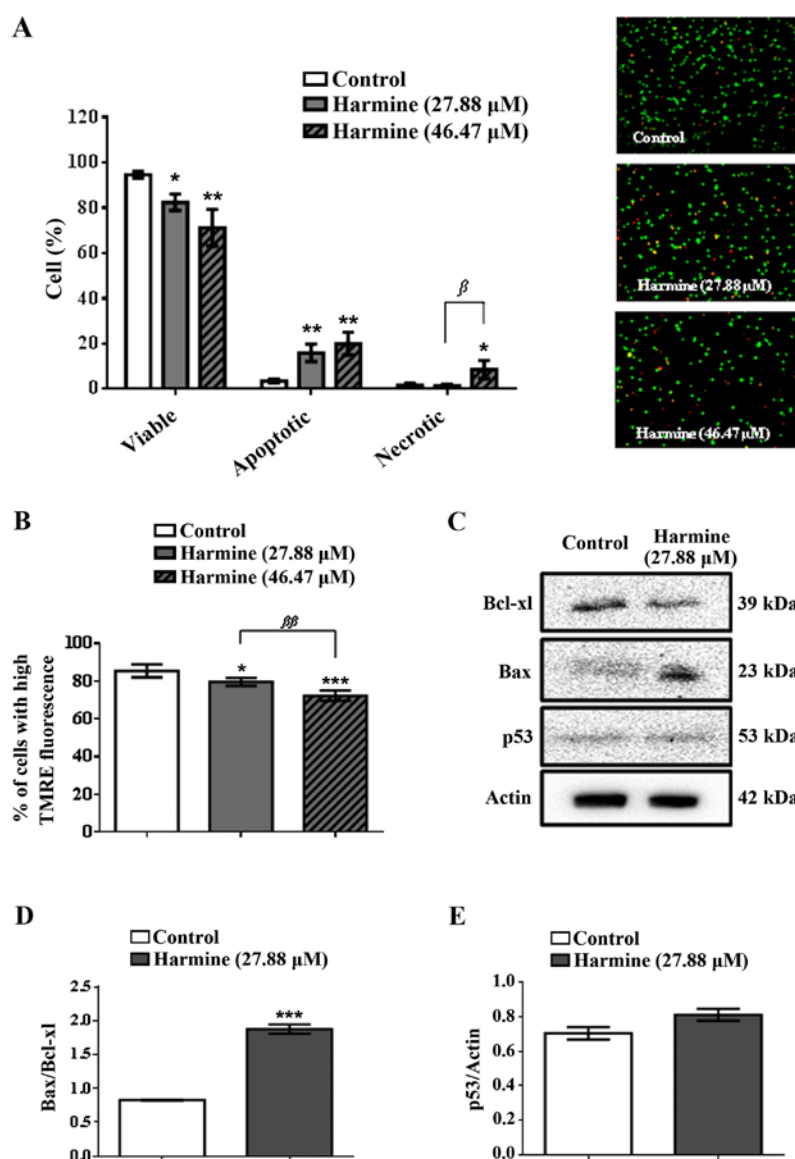
Figure 2. (A) Morphology of MCF-7 cells and the type of cell death induced by harmine (27.88 and 46.47 μM, 72 h), evaluated by a staining method with propidium iodide and acridine orange and visualized by fluorescence microscopy (x400); red, orange and green stains denote necrotic, apoptotic and viable cells, respectively. (B) Effects of harmine (27.88 and 46.47 μM, 48 h) on the mitochondrial membrane potential ($\Delta\Psi$m) of MCF-7 cells. (C-E) Imunoblotting and quantitative data of proteins that modulate apoptosis (Bcl-xL, Bax and p53) of MCF-7 cells treated with harmine (27.88 μM, 48 h). Results are expressed as the means ± standard deviation of three independent experiments. Data were analysed by analysis of variance one-way ANOVA and Bonferroni test. *, ** and *** denote statistical differences compared to negative control data, when $P<0.05$, $P<0.01$ and $P<0.001$, respectively. $^\beta$ and $^{\beta\beta}$ denote statistical differences comparing the concentration of 27.88 μM to 46.47 μM harmine, with $P<0.05$ and $P<0.01$.

by AutoDock Vina (-7.6 kcal/mol; RMSD 0.00000) after submission to MD simulations (1 ns), showed harmine to be intercalated between the hydrophobic portions of nucleotide residues dt620 and dt619 in the strand B of DNA (Fig. 5A). The frame correspondent to 10 ps showed one H-bond between the harmine donor atom N14, which shares the H atom (H15) with the acceptor atom (O4') of residue dt620 (2.007 Å) (Fig. 5A), although this H-bond presents only 2.8% occupancy. Fig. 5B (bottom) also has other H-bonds, which act as acceptors to nucleotides dt619 (0.4%) and da606 (0.2%). The nucleotide da606, however, formed one H-bond with harmine (0.2%) and, for this reason, acted as an H-bond donor. Additionally, variations in the RMSD of harmine (Fig. 5B, insert) indicated an initial stability of the complex that was briefly maintained by H-bonding. Probably fluctuations of RMSD (~5Å) come from

the DNA-harmine hydrophobic interactions (residues da605, da606, dt619 and dt620) initially predicted by AutoDock Vina (Fig. S1A), which had the highest hydrophobic contribution value (11.78219) among other predicted poses of harmine. The same hydrophobic interactions remain after MD simulations (Fig. 5C). Additionally, the H-bonds predicted by GROMACS showed a predominance of pairs with distances of up to 3.5Å (Fig. S2A), confirming the H-bond distance progression variations of close to 3.5Å (Fig. S2B). Indeed, the H-bond angle distribution from the ideal of 150° to a less favourable angle (50°) (Fig. S2C) confirmed the minor role of H-bonds in the maintenance of harmine inside the DNA hydrophobic cavity.

The MM-PBSA method predicted some energies in the full DNA-harmine complex. The non-ligated potential corresponding to van der Waals energy was -121.93±0.81 kJ/mol,
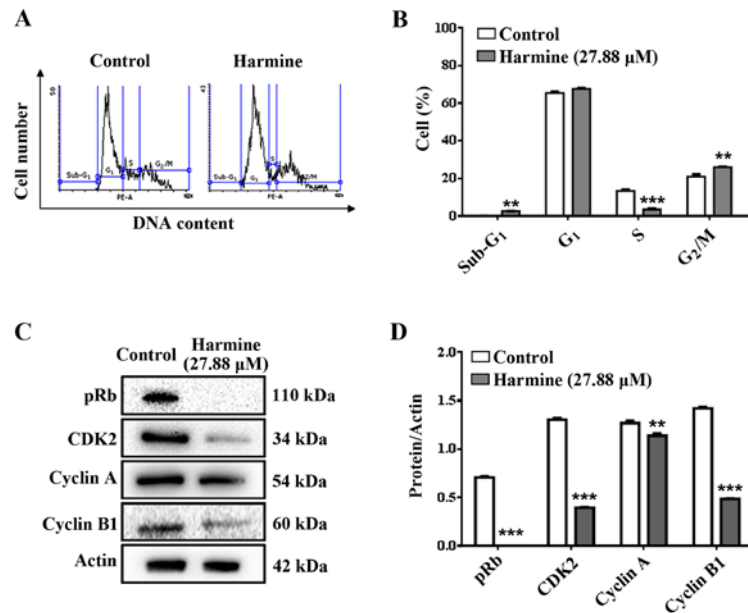
Figure 3. (A) Histogram and (B) percentages of MCF-7 cells in each phase of the cell cycle (Sub-G_1, G_1, S and G_2/M). Cells were treated with harmine (27.88 μM, 72 h) and analysed by flow cytometry. (C) Imunoblotting and (D) Quantitative data of regulatory proteins of the cell cycle; pRb, CDK2, cyclin A and cyclin B1, respectively, in MCF-7 cells treated with harmine (27.88 μM, 48 h). Sub-G_1: Debris and dead cells; G_1: cells not presenting DNA duplication; S: cells presenting intermediate DNA content; G_2/M: cells presenting duplicated DNA. Results are expressed as the means ± standard deviation of three independent experiments. Data were analysed by analysis of variance one-way ANOVA and Bonferroni test. ** and *** denote statistical differences compared to the negative control, when P<0.01 and P<0.001, respectively.
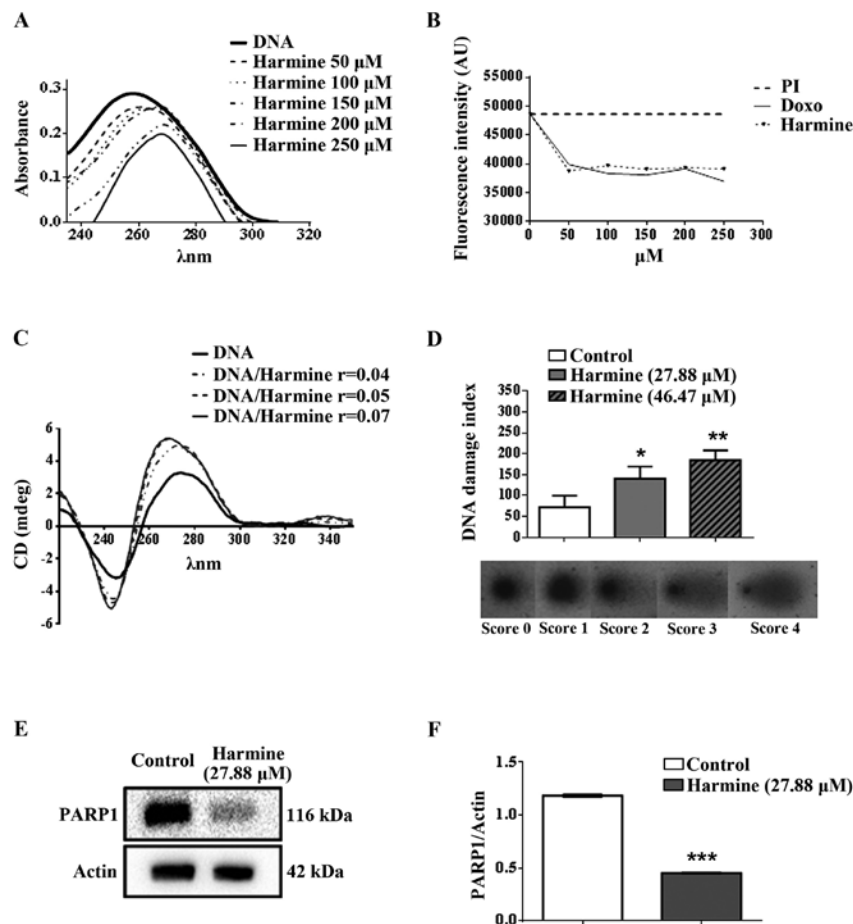

Figure 4. Effects of harmine on calf thymus DNA (CT-DNA, 150 μM) evaluated by (A) UV-visible spectroscopy, (B) Fluorescence spectroscopy and (C) Circular dichroism approach. (D) DNA damage index analysed by Comet assay. (E) Imunoblotting and (F) Quantitative data of the PARP1 protein, involved in DNA repair, evaluated in MCF-7 cells treated with harmine (27.88 μM, 48 h). The results are expressed as the means ± standard deviation of three independent experiments. Data were analysed by analysis of variance one-way ANOVA and Bonferroni test. *, ** and *** denote statistical differences compared to data of the negative control, when P<0.05, P<0.01 and P<0.001, respectively.
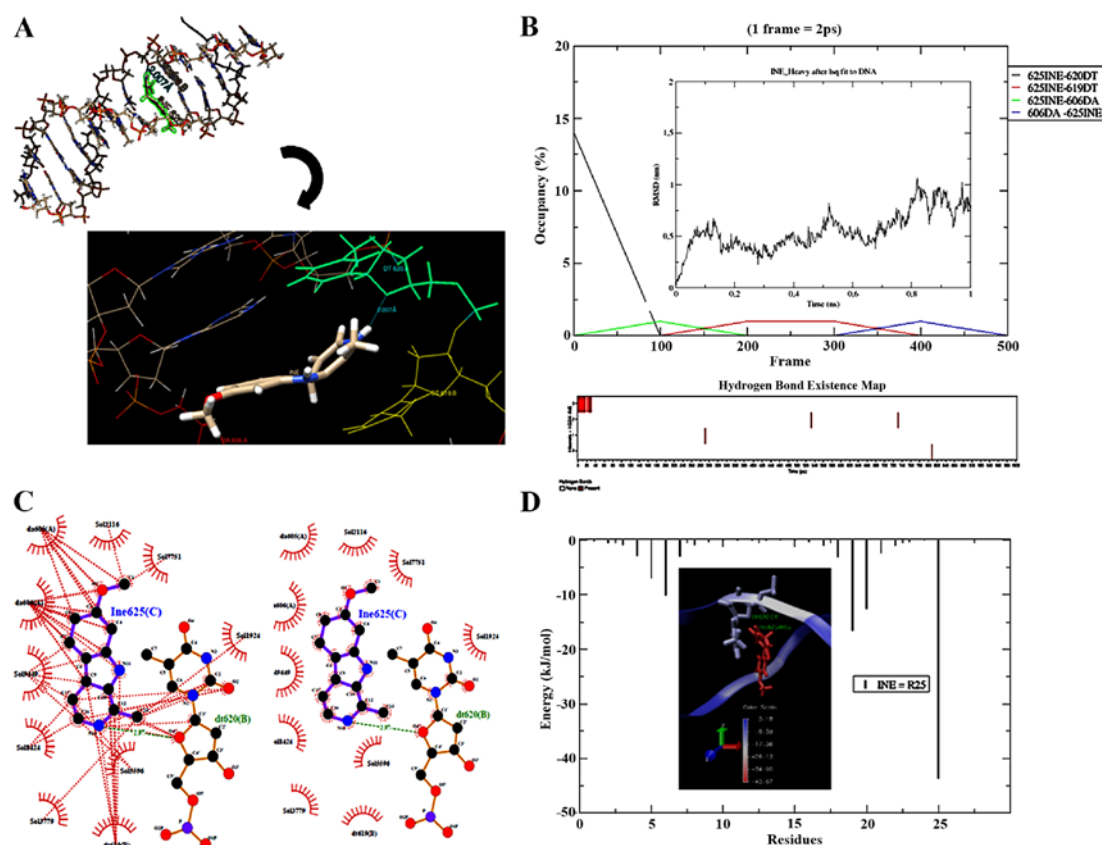
Figure 5. MD simulations showed harmine interactions with nucleotides of DNA (PDB 1G3X): (A) Harmine intercalated (highlighted in green) and formed one H-bond with nucleotide (dt620). (B) H-bonds occupancy rate (each frame=2 ps) for each nucleotide reflects harmine RMSD variations. (C) Dashed red lines depict hydrophobic interactions and dashed green lines represent one H-bond formed between harmine and DNA nucleotides. (D) Each nucleotide of DNA (1-24) and ligand (harmine) (25) had specific contributions to the total energy. Inserted complex image shows colour score related to the contribution energies of each residue, where the lowest contribution comes from harmine (red) H-bonded to dt620 (blue). INE, harmine.

Treatments (mg/kg/day)	Variation of Body weight (g)	Volume of ascitic fluid (ml)	Volume of packed cells (ml)
Control	9.84±1.04	10.76±1.91	3.60±0,49
Harmine 10	6.94±0.85 *	6.50±2.83 *	2.50±0,71
Harmine 20	6.45±0.80 **	6.03±1.88 **	2.13±0.65 *
Doxorubicin 0.6	5.38±1.03 ***	2.79±1.28 ***	1.29±0.58 ***

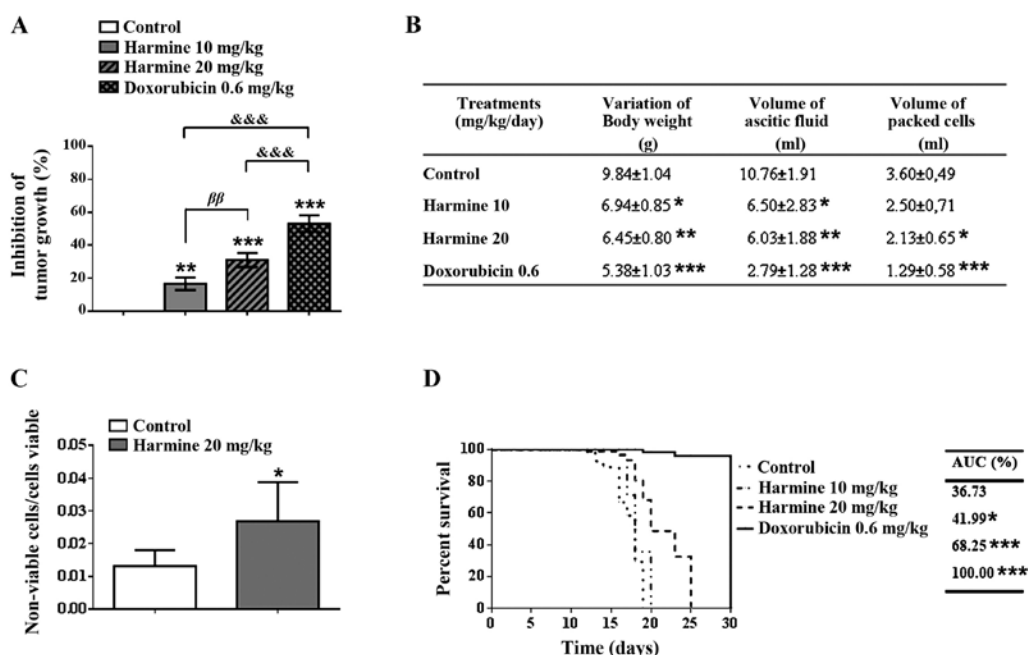|	AUC (%)
Control	36.73
Harmine 10 mg/kg	41.99*
Harmine 20 mg/kg	68.25 ***
Doxorubicin 0.6 mg/kg	100.00 ***

Figure 6. Antitumor effect of harmine (10 and 20 mg/kg/day, 9 days) in male Balb/c mice bearing Ehrlich ascitic carcinoma (EAC) cells. (A) Inhibition of tumour growth, based on the variation in abdominal circumference. (B) Body weight, volume of ascitic fluid and volume of packed tumour cells in mice treated with harmine. (C) Viability of EAC cells assessed by trypan blue assay. (D) Survival rate of mice treated with harmine, according to the Kaplan-Meier method. The results are expressed as the means ± standard deviation of biological replication, n=12. Data were analysed by analysis of variance one-way ANOVA followed by Bonferroni test or log-rank test, when necessary. *, ** and *** denote statistical differences compared to data of the negative control, when P<0.05, P<0.01 and P<0.001, respectively. $^{\beta\beta}$ denote statistical differences comparing mice that received 10 mg/kg/day to those that received 20 mg/kg/day (P<0.01). $^{\&\&\&}$ denote statistical differences compared to the positive control (P<0.001).

while the electrostatic energy was 14.55±0.28 kJ/mol. The value of complex binding energy (-106.42±0.82 kJ/mol) corresponded to the polar solvation energy (14.54±0.28 kJ/mol) and non-polar solvation energy related to the Solvent Accessible Surface Area (SASA) (-10.55±0.06 kJ/mol) plus molecular mechanic energy (Fig. S2D). Additionally, MM-PBSA calculated the van der Waals energy that represented the main contribution to the molecular energy of the complex at vacuum (Fig. S2E). The interior of the harmine complex had the lowest energy value, which contributed to its total energy (Fig. 5D). Harmine also interacted with the water molecules associated with the solvation shell (Fig. 5C). Finally, explicit solvent modelling (TIP3P) from GROMACS simulations allowed MM-PBSA to calculate the DNA-harmine complex SASA Free Energy of Solvation (ΔGsolv) (Fig. S2F). The ΔGsolv was maintained at approximately -44 kJ/mol throughout the assay. This confirmed that the energy required to move harmine from the aqueous solvent to the non-polar environment (DNA) was very low, which favoured the DNA-harmine interactions.

Harmine induces DNA damage and decreases the expression of PARP1. After treating MCF-7 cells with 27.88 or 46.47 μM, harmine caused DNA damage indexes of 140.61±28.66 and 184.35±23.66%, respectively, while the negative control index was 72.26±27.72% (Fig. 4D). In addition, 27.88 and 46.47 μM harmine increased DNA damage in MCF-7 cells by 48.6 and 60.8% respectively, when compared to the untreated cells.

Furthermore, harmine (27.88 μM, 48 h) significantly decreased the expression of PARP1 (Fig. 4E and F), suggesting a possible reduction of the PARP1-dependent DNA repair mechanism.

Harmine inhibits tumour growth and increases animal lifespan. The treatment of Balb/c mice with harmine was able to significantly inhibit tumour growth, in a dose-dependent manner, compared to the negative control (Fig. 6A). At the concentration of 10 mg/kg/day, harmine inhibited tumour growth by 16.77±3.88%, whereas the concentration of 20 mg/kg/day had a significantly greater effect, inhibiting tumour growth by 31.10±4.19%. Doxorubicin (0.6 mg/kg/day) used as a positive control was able to inhibit tumour growth by 53.20±5.02%.

Harmine also reduced significantly the variation of body weight and the volume of ascitic fluid, in a dose-dependent manner, when compared to the negative control. However, it is noted that only harmine at concentration of 20 mg/kg/day was able to decrease significantly the volume of packed tumour cells (2.13±0.65), compared to the negative control (3.60±0.49) (Fig. 6B). Furthermore, the proportion of non-viable/viable tumour cells increased when the treatment was done with 20 mg/kg/day of harmine (Fig. 6C). Doxorubicin (0.6 mg/kg/day) also reduced significantly the evaluated parameters.

The effect of harmine on mouse lifespan was evaluated using the method of Kaplan and Meier (1958) (Fig. 6D). Animals receiving 10 mg/kg/day of harmine demonstrated a small prolongation of lifespan (42.0%), when compared to the negative control group (36.7%). In contrast, animals receiving 20 mg/kg/day of harmine presented a significantly longer lifespan (68.3%), when compared with the negative control. No mortality occurred in animals treated with doxorubicin (0.6 mg/kg/day).

Discussion

The selective cytotoxic effect to MCF-7 and HeLa cells was clearly observed in the treatment with harmine at different treatment times. The SI demonstrates the potential of a compound to target tumour cell lines preferentially, instead of normal cell lines (48). Therefore, a SI value of greater than two indicates low toxicity for normal cells and high toxicity against tumour cell lines. Observing the results harmine showed a higher selectivity to the MCF-7 cells, where SI values of 3.25 and 4.44 were obtained in 48 and 72 h of treatment, respectively.

Harmine was able to induce significant cell death in MCF-7 cells, which could be associated with an increase in the numbers of apoptotic and necrotic cells, while decreasing the numbers of viable cells. Furthermore, it was capable of decreasing the mitochondrial membrane potential ($\Delta\Psi$m) in a dose-dependent manner. In this regard, it is already known that $\Delta\Psi$m, which is established by the proton pumps of the electron transport chain, is crucial for mitochondrial function. Loss of $\Delta\Psi$m can decrease ATP generation and Ca^{2+} uptake, in addition to triggering the apoptotic process for being related to the transient activation of the mitochondrial permeability transition pore, in which diverse pro-apoptotic proteins are released from the mitochondria into the cytoplasm, e.g., cytochrome c and Bax (49-51). The results obtained by the assays of the type of cell death and mitochondrial depolarization corroborate each other. Therefore, our findings suggest that harmine caused mitochondrial dysfunction, accompanied by a loss of mitochondrial membrane potential and induced cell death via apoptosis.

Bcl-2 family proteins are key regulators of apoptosis via the mitochondrial pathway. Proteins such as Bcl-2 and Bcl-xL prevent apoptosis, whereas proteins associated to Bcl-2, such as Bax and Bak, promote apoptosis (52). The results showed that harmine significantly increased the Bax/Bcl-xL ratio, suggesting cell death through apoptosis via the mitochondrial pathway. Such findings confirmed previous results regarding the type of cell death and mitochondrial depolarization. However, it should be noted that harmine induced apoptotic cell death independently of p53. Luo and collaborators (53) observed similar results in a human colon cancer cell line treated with the anti-cancer compound methoxy-1-styryl-9*H*pyrido-[3,4-b]-indole (JKA97), a synthetic harmine analogue. Their results demonstrated that JKA97-inducing cell death occurred via the Bax-dependent and p53-independent pathway.

By assessing the effect of harmine on each phase of the cell cycle in MCF-7 cells, it was possible to verify that harmine had the ability to promote a significant decrease in the number of cells in the S phase, while significantly increasing the number of cells in the G_2/M phase, thereby suggesting a G_2/M arrest of cells. In fact, cancer cells exhibiting a faulty G_1 checkpoint due to loss of p53 or pRb may show a greater sensitivity to G_2/M checkpoint inhibitors. This allows cells with damaged DNA to enter through aberrant mitosis and undergo apoptosis. Additionally, the ability of harmine to cause cell cycle arrest

at G_2/M could be indicative of its inhibitory effect on proteins involved in cell cycle regulation.

Each stage of the cell cycle is tightly regulated by cyclin-dependent kinases (CDKs) and their regulatory partners cyclins, which are expressed in a periodic manner. Activated CDKs phosphorylate several key substrates that promote cell cycle progression (54). Upon mitogenic stimuli, the cells receive signals to enter the G1 phase and initiate the cell cycle progression. Subsequently, CDK4/CDK6/cyclin D and cyclin E/CDK2 complexes initiate a phosphorylation cascade of retinoblastoma protein (RB1, also known as p105-RB) with consequent dissociation of the entire repressive complex (RB1-E2F). This inactivates the function of protein RB1 (pRb) as a transcriptional repressor and enables E2F transcription factors (E2Fs) to increase the transcription of genes involved in cell cycle progression, notably CDK2, cyclin A and cyclin B proteins. Finally, cyclin A/CDK2, cyclin A/CDK1 and cyclin B/CDK1 complexes become responsible for keeping pRb in a hyperphosphorylated state until the end of cell cycle (55). Consequently, inactivation of pRb and permanent activation of E2F can cause unrestrained proliferation. Harmine was capable of totally inhibiting pRb phosphorylation, which suggests that pRb was fully activated and repressing the E2F transcription factors, thereby leading to decreased expression of various regulatory proteins of the cell cycle, in such a way demonstrating the pRb anti-proliferative function. Furthermore, harmine caused a significant decrease in the cell cycle proteins, CDK2, cyclin A and cyclin B1, confirming the results regarding the significant reduction of cells present in the S phase and cell cycle arrest at the G_2/M phase. It is well known that the cyclin E/CDK2 complex regulates G_1/S phase transition, whereas the cyclin A/CDK2 complex is required during the S phase. The cyclin A/CDK1 complex regulates G_2/M phase transition, while the cyclin B/CDK1 complex regulates the M phase progression (54).

It is important to point out here that harmine caused an intense inhibition of the S phase (73.7%) in the MCF-7 cells. This S phase inhibitory effect could arise from the synergistic effect of pRb anti-proliferative function, which decreased CDK2 expression and is also due to the fact that harmine is an ATP-competitive CDK inhibitor (56).

Hilgendorf and collaborators (57) reported that pRb can promote DNA damage-induced apoptosis in the highly proliferative tumour cells by transcriptionally co-activating pro-apoptotic genes, such as caspase 7 and p73. Moreover, pRb can also directly bind to and activate Bax protein. These findings indicate that both the transcriptional as well as the mitochondrial pro-apoptotic functions of pRb occurred independently of p53, thereby corroborating our results.

Depending on how severe the DNA damage is, the basic molecular mechanisms of the response against DNA damage can switch between cell-cycle arrest (giving the appropriate cell time to attempt the repair of the DNA lesion) to induction of death programs, such as apoptosis or necrosis (58). As DNA damage can induce cell-cycle arrest and/or cell death, DNA is an important molecular target of many antitumor agents (59).

To achieve a greater understanding regarding the binding of harmine to DNA, we investigated the DNA-harmine interaction. Firstly, the results of UV-Visible spectroscopy suggested that harmine binds to CT-DNA by intercalation, since harmine caused a hypochromic and bathochromic effect. According to Villanueva and collaborators (47), hypochromic and bathochromic effects are evidence of stacking interactions between conjugated aromatic systems that intercalate within the DNA nucleobases. The chemical structure of harmine is characterized by a pyridine ring fused to an indolyl ring, besides a methyl group and a methoxy group at positions 1 and 7, respectively (60). As such, the molecular geometry of harmine (tricyclic planar) facilitates its binding to DNA by intercalation.

The ability of harmine to intercalate between DNA nucleobases was further confirmed by fluorescence spectroscopy and CD spectroscopy. The results from molecular simulation indicated that van der Waals and hydrophobic interactions, plus the water solvation-harmine interactions, facilitated its binding into the adenine-thymine specific DNA structure by intercalation. Molecular docking confirmed the hypochromic and bathochromic effects of harmine, as well as displacement of intercalated PI and CD spectrum changes, which proved experimentally that harmine indeed intercalated between subsequent nucleobase pairs of DNA. Finally, harmine caused significant DNA damage in MCF-7 cells in a dose-dependent manner, which confirmed the results obtained from spectrometry and molecular simulation.

Structural DNA damage triggers a variety of DNA repair mechanisms, collectively termed DNA damage response (DDR), and one of the pillars of DDR is the activity of poly (adenosine diphosphate ribose) polymerase (PARP) (61). PARP1, one of the best-studied members of this family of enzymes, is overexpressed in a variety of cancers. Its expression has been linked to the poor prognosis of cancers, most notably breast cancer (62). Our results showed that harmine significantly decreased the expression of PARP1, indicating that it has the ability to decrease the PARP1-dependent DNA repair mechanism, in addition to inducing DNA damage itself.

According to Cseh and collaborators (61), PARP1 has another function beyond DNA repair; i.e., PARP-1 controls the integrity and function of mitochondria, a critical source of PARP-1 co-enzyme NAD^+. Among other important nuclear-encoded mitochondrial genes, PARP-1 contributes to the trans-activation of genes that encode critical components of the mitochondrial electron transport chain, such as cytochrome c and complex I subunit NADH dehydrogenase 2 (ND2). Thus, it is possible that the loss of $\Delta\Psi$m observed in MCF-7 cells treated with harmine may occur, at least in part, due to the decrease in PARP1 expression, also contributing to the cell death by apoptosis. However, more studies are necessary to further elucidate this hypothesis.

Finally, after the evaluation of the *in silico* and *in vitro* cytotoxic effects of harmine, we determined its antitumour activity *in vivo*, using Balb/c mice bearing Ehrlich ascitic carcinoma (EAC). Accordingly, harmine was able to significantly inhibit the tumour growth besides decreasing the variation of body weight, volume of ascitic fluid and volume of packed tumour cells. Moreover, harmine increased the proportion of non-viable/viable tumour cells, which consequently increased the lifespan of treated animals, thus demonstrating its antitumour effects *in vivo*. It should be also noted that, based on our search of the related literature, this is the first report of the effects of the β-carboline alkaloid harmine on the EAC model.

In conclusion, the current study identified that the β-carboline alkaloid harmine has a cytotoxic selective effect to tumour cell

lines. In addition, our findings showed that harmine intercalated between nucleobase pairs of DNA rich in adenine-thymine, induced a dose-dependent DNA damage and decreasing the PARP1-dependent DNA repair mechanism, which caused cell cycle arrest at the G_2/M phase via inhibition of phosphorylation of pRb and reduction of the expression of CDK2, cyclin A and cyclin B1. Harmine also induced mitochondrial-related cellular apoptosis by modulating the expression of Bcl-2 family proteins and decreasing the mitochondrial membrane potential. Moreover, harmine presented *in vivo* antitumour effects on Balb/c mice bearing Ehrlich ascitic carcinoma. Taken together, the results suggest that harmine, present in the pulp and seed of the passion fruit, could be used in the future as a promising coadjutant anticancer agent. In addition, we suggest to address this fruit as a functional food.

Acknowledgements

Availability of data and materials

Not applicable.

Authors' contributions

NSRSM, TS and GMA performed the *in vitro* assays. CTP performed the circular dichroism DNA interaction assay. The other DNA interaction assays were performed by NSRSM. VMASG performed the *in silico* simulation (AutoDock Vina and GROMACS). NSRSM and KBF performed the western blotting. NSRSM and RCZ performed the *in vivo* assays. RCP designed the research and revised the manuscript. MRK and DWF also revised the manuscript. All authors read and approved the final manuscript.

Ethics approval and consent to participate

All animal procedures were carried out according to internationally accepted principles for laboratory animal use and care (NIH publication no. 85-23, revised in 1985). The experimental protocol received approval from the ethics committee of the Universidade Federal de Santa Catarina, Brazil (CEUA-PP00784).

Patient consent for publication

Not applicable.

Competing interests

The authors declare that they have no competing interests.

References

1. World Health Organization (WHO): Cancer. WHO, Geneva, 2018. https://www.who.int/cancer/en/. Accessed September 12, 2018.
2. Ali R, Mirza Z, Ashraf GMD, Kamal MA, Ansari SA, Damanhouri GA, Abuzenadah AM, Chaudhary AG and Sheikh IA: New anticancer agents: Recent developments in tumor therapy. Anticancer Res 32: 2999-3005, 2012.
3. Patel K, Gadewar M, Tripathi R, Prasad SK and Patel DK: A review on medicinal importance, pharmacological activity and bioanalytical aspects of beta-carboline alkaloid 'Harmine'. Asian Pac J Trop Biomed 2: 660-664, 2012.
4. Piechowska P, Zawirska-Wojtasiak R and Mildner-Szkudlarz S: Bioactive β-carbolines in food: a review. Nutrients 11: 1-10, 2019.
5. Tsuchiya H, Shimizu H and Iinuma M: Beta-carboline alkaloids in crude drugs. Chem Pharm Bull (Tokyo) 47: 440-443, 1999.
6. Li S, Teng L, Liu W, Cheng X, Jianga B, Wang Z and Wang CH: Pharmacokinetic study of harmane and its 10 metabolites in rat after intravenous and oral administration by UPLC-ESI-MS/MS. Pharm Biol 54: 1768-1781, 2016.
7. Pierson JT, Dietzgen RG, Shaw PN, Roberts-Thomson SJ, Monteith GR and Gidley MJ: Major Australian tropical fruits biodiversity: Bioactive compounds and their bioactivities. Mol Nutr Food Res 56: 357-387, 2012.
8. Lam SK and Ng TB: Passiflin, a novel dimeric antifungal protein from seeds of the passion fruit. Phytomedicine 16: 172-180, 2009.
9. Ingale AG and Hivrale AU: Pharmacological studies of *Passiflora* sp. and their bioactive compounds. Afr J Plant Sci 4: 417-426, 2010.
10. Zhang P, Huang CR, Wang W, Zhang XK, Chen JJ, Wang JJ, Lin C and Jiang JW: Harmine hydrochloride triggers G2 phase arrest and apoptosis in MGC-803 cells and SMMC-7721 cells by upregulating p21, activating caspase-8/Bid, and downregulating ERK/Bad pathway. Phytother Res 30: 31-40, 2016.
11. Sobhani AM, Ebrahimi SA and Mahmoudian M: An in vitro evaluation of human DNA topoisomerase I inhibition by *Peganum harmala* L. seeds extract and its β-carboline alkaloids. J Pharm Pharm Sci 5: 19-23, 2002.
12. Liu J, Li Q, Liu Z, Lin L, Zhang X, Cao M and Jiang J: Harmine induces cell cycle arrest and mitochondrial pathway-mediated cellular apoptosis in SW620 cells via inhibition of the Akt and ERK signaling pathways. Oncol Rep 35: 3363-3370, 2016.
13. Hamsa TP and Kuttan G: Harmine activates intrinsic and extrinsic pathways of apoptosis in B16F-10 melanoma. Chin Med 6: 11, 2011.
14. Mosmann T: Rapid colorimetric assay for cellular growth and survival: Application to proliferation and cytotoxicity assays. J Immunol Methods 65: 55-63, 1983.
15. Koch A, Tamez P, Pezzuto J and Soejarto D: Evaluation of plants used for antimalarial treatment by the Maasai of Kenya. J Ethnopharmacol 101: 95-99, 2005.
16. McGahon AJ, Martin SJ, Bissonnette RP, Mahboubi A, Shi Y, Mogil RJ, Nishioka WK and Green DR: The end of the (cell) line: Methods for the study of apoptosis in vitro. Methods Cell Biol 46: 153-185, 1995.
17. O'Reilly CM, Fogarty KE, Drummond RM, Tuft RA and Walsh JV Jr: Quantitative analysis of spontaneous mitochondrial depolarizations. Biophys J 85: 3350-3357, 2003.
18. Navarro M, Cisneros-Fajardo EJ, Fernandez-Mestre M, Arrieche D and Marchan E: Synthesis, characterization, DNA binding study and biological activity against Leishmania mexicana of [Cu(dppz)2]BF4. J Inorg Biochem 97: 364-369, 2003.
19. Da Silveira VC, Benezra H, Luz JS, Georg RC, Oliveira CC and Ferreira AMDC: Binding of oxindole-Schiff base copper (II) complexes to DNA and its modulation by the ligand. J Inorg Biochem 105: 1692-1703, 2011.
20. Bertoldo JB, Razzera G, Vernal J, Brod FCA, Arisi ACM and Terenzi H: Structural stability of Staphylococcus xylosus lipase is modulated by Zn(2+) ions. Biochim Biophys Acta 1814: 1120-1126, 2011.
21. Malinina L, Soler-López M, Aymamí J and Subirana JÁ: Intercalation of an acridine-peptide drug in an AA/TT base step in the crystal structure of [d(CGCGAATTCGCG)]|(2) with six duplexes and seven Mg(2+) ions in the asymmetric unit. Biochemistry 41: 9341-9348, 2002.

22. Pettersen EF, Goddard TD, Huang CC, Couch GS, Greenblatt DM, Meng EC, Ferrin TE and Ferrin TE: UCSF Chimera - a visualization system for exploratory research and analysis. J Comput Chem 25: 1605-1612, 2004.

23. Hornak V, Abel R, Okur A, Strockbine B, Roitberg A and Simmerling C: Comparison of multiple AMBER force fields and development of improved protein backbone parameters. Proteins 65: 712-725, 2006.

24. Sousa da Silva AW and Vranken WF: ACPYPE - AnteChamber PYthon Parser interfacE. BMC Res Notes 5: 367, 2012.

25. Wang J, Wang W, Kollman PA and Case DA: Automatic atom type and bond type perception in molecular mechanical calculations. J Mol Graph Model 25: 247-260, 2006.

26. Forli S, Huey R, Pique ME, Sanner MF, Goodsell DS, Olson AJ and Olson AJ: Computational protein-ligand docking and virtual drug screening with the AutoDock suite. Nat Protoc 11: 905-919, 2016.

27. Trott O and Olson AJ: AutoDock Vina: Improving the speed and accuracy of docking with a new scoring function, efficient optimization, and multithreading. J Comput Chem 31: 455-461, 2010.

28. Schrödinger LCC: The PyMOL Molecular Graphics System, Version 1.8. Schrödinger. LCC, New York, NY, 2015.

29. Laskowski RA and Swindells MB: LigPlot+: Multiple ligand-protein interaction diagrams for drug discovery. J Chem Inf Model 51: 2778-2786, 2011.

30. Hanwell MD, Curtis DE, Lonie DC, Vandermeersch T, Zurek E and Hutchison GR: Avogadro: An advanced semantic chemical editor, visualization, and analysis platform. J Cheminform 4: 17, 2012.

31. Van Der Spoel D, Lindahl E, Hess B, Groenhof G, Mark AE and Berendsen HJC: GROMACS: Fast, Flexible, and Free. J Comput Chem 26: 1701-1718, 2005.

32. Abraham M, Hess B, Van Der Spoel D, Lindahl E and the GROMACS development team: GROMACS User Manual version 4, 2018. www.gromacs.org.

33. Jorgensen WL, Chandrasekhar J, Madura JD, Impey RW and Klein ML: Comparison of simple potential functions for simulating liquid water. J Chem Phys 79: 926-935, 1983.

34. Kumari R, Kumar R and Lynn A; Open Source Drug Discovery Consortium: g_mmpbsa - a GROMACS tool for high-throughput MM-PBSA calculations. J Chem Inf Model 54: 1951-1962, 2014.

35. Hsin J, Arkhipov A, Yin Y, Stone JE and Schulten K: Using VMD: an introductory tutorial. Curr Protoc Bioinformatics: CHAPTER: Unit–5.7, 2008.

36. Verlet L: Computer 'Experiments' on Classical Fluids. I. Thermodynamical Properties of Lennard-Jones Molecules. Phys Rev 159: 98-103, 1967.

37. Lemkul JA, Allen WJ and Bevan DR: Practical considerations for building GROMOS-compatible small-molecule topologies. J Chem Inf Model 50: 2221-2235, 2010.

38. Singh NP, McCoy MT, Tice RR and Schneider EL: A simple technique for quantitation of low levels of DNA damage in individual cells. Exp Cell Res 175: 184-191, 1988.

39. Ross GM, McMillan TJ, Wilcox P and Collins AR: The single cell microgel electrophoresis assay (comet assay): Technical aspects and applications. Report on the 5th LH Gray Trust Workshop, Institute of Cancer Research, 1994. Mutat Res 337: 57-60, 1995.

40. Laemmli UK: Cleavage of structural proteins during the assembly of the head of bacteriophage T4. Nature 227: 680-685, 1970.

41. Kviecinski MR, Benelli P, Felipe KB, Correia JFG, Pich CT, Ferreira SRS and Pedrosa RC: SFE from *Bidens pilosa* Linné to obtain extracts rich in cytotoxic polyacetilenes with antitumor activity. J Supercrit Fluids 56: 243-248, 2011.

42. Hossain MA, Kim D, Jang JY, Kang YJ, Yoon JH, Moon JK, Chung HY, Kim GY, Choi YH, Copple BL and Kim ND: Aspirin enhances doxorubicin-induced apoptosis and reduces tumor growth in human hepatocellular carcinoma cells *in vitro* and *in vivo*. Int J Oncol 40: 1636-1642, 2012.

43. Felipe KB, Kviecinski MR, Ourique F, Bücker NF, Farias MS, Castro LSEPW, Grinevicius VMAS, Motta NS, Correia JFG, Rossi MH and Pedrosa RC: Inhibition of tumor proliferation associated with cell cycle arrest caused by extract and fraction from *Casearia sylvestris* (Salicaceae). J Ethnopharmacol 155: 1492-1499, 2014.

44. Kaplan EL and Meier P: Nonparametric estimation from incomplete observations. J Am Stat Assoc 53: 457-481, 1958.

45. Strober W: Trypan blue exclusion test of cell viability. Curr Protoc Immunol 3 (Appendix): 3B, 2001.

46. Fox K: Drug-DNA interaction protocols. 2nd edition. Humana Press, Southampton, 1977.

47. Villanueva PJ, Martinez A, Baca ST, DeJesus RE, Larragoity M, Contreras L, Gutierrez DA, Varela-Ramirez A and Aguilera RJ: Pyronaridine exerts potent cytotoxicity on human breast and hematological cancer cells through induction of apoptosis. PLoS One 13: e0206467, 2018.

48. Badisa RB, Darling-Reed SF, Joseph P, Cooperwood JS, Latinwo LM and Goodman CB: Selective cytotoxic activities of two novel synthetic drugs on human breast carcinoma MCF-7 cells. Anticancer Res 29: 2993-2996, 2009.

49. Duchen MR: Contributions of mitochondria to animal physiology: From homeostatic sensor to calcium signalling and cell death. J Physiol 516: 1-17, 1999.

50. Tan ML, Ooi JP, Ismail N, Moad AI and Muhammad TS: Programmed cell death pathways and current antitumor targets. Pharm Res 26: 1547-1560, 2009.

51. Nakagawa Y, Suzuki T, Ishii H, Ogata A and Nakae D: Mitochondrial dysfunction and biotransformation of β-carboline alkaloids, harmine and harmaline, on isolated rat hepatocytes. Chem Biol Interact 188: 393-403, 2010.

52. Brown R: The bcl-2 family of proteins. Br Med Bull 53: 466-477, 1997.

53. Luo W, Liu J, Li J, Zhang D, Liu M, Addo JK, Patil S, Zhang L, Yu J, Buolamwini JK, *et al*: Anti-cancer effects of JKA97 are associated with its induction of cell apoptosis via a Bax-dependent and p53-independent pathway. J Biol Chem 283: 8624-8633, 2008.

54. Bai J, Li Y and Zhang G: Cell cycle regulation and anticancer drug discovery. Cancer Biol Med 14: 348-362, 2017.

55. Johnson J, Thijssen B, McDermott U, Garnett M, Wessels LFA and Bernards R: Targeting the RB-E2F pathway in breast cancer. Oncogene 35: 4829-4835, 2016.

56. Song Y, Kesuma D, Wang J, Deng Y, Duan J, Wang JH and Qi RZ: Specific inhibition of cyclin-dependent kinases and cell proliferation by harmine. Biochem Biophys Res Commun 317: 128-132, 2004.

57. Hilgendorf KI, Leshchiner ES, Nedelcu S, Maynard MA, Calo E, Ianari A, Walensky LD and Lees JA: The retinoblastoma protein induces apoptosis directly at the mitochondria. Genes Dev 27: 1003-1015, 2013.

58. Surova O and Zhivotovsky B: Various modes of cell death induced by DNA damage. Oncogene 32: 3789-3797, 2013.

59. Hurley LH: DNA and its associated processes as targets for cancer therapy. Nat Rev Cancer 2: 188-200, 2002.

60. Pagano B, Caterino M, Filosa R and Giancola C: Binding of Harmine Derivatives to DNA: A Spectroscopic Investigation. Molecules 22: 1831, 2017.

61. Cseh AM, Fábián Z, Sümegi B and Scorrano L: Poly(adenosine diphosphate-ribose) polymerase as therapeutic target: Lessons learned from its inhibitors. Oncotarget 8: 50221-50239, 2017.

62. Rojo F, García-Parra J, Zazo S, Tusquets I, Ferrer-Lozano J, Menendez S, Eroles P, Chamizo C, Servitja S, Ramírez-Merino N, *et al*: Nuclear PARP-1 protein overexpression is associated with poor overall survival in early breast cancer. Ann Oncol 23: 1156-1164, 2012.